Mass distribution and mass resolved angular distribution of fission products in $^{28}Si + ^{232}Th$

Suparna Sodaye,[1,*] R. Tripathi,[1] B. V. John,[2] K. Ramachandran,[2] and P. K. Pujari[1]
[1]*Radiochemistry Division, Bhabha Atomic Research Centre, Trombay, Mumbai 400 094, India*
[2]*Nuclear Physics Division, Bhabha Atomic Research Centre, Trombay, Mumbai 400 094, India*
(Received 11 November 2016; published 26 January 2017)

Background: Fission process with heavier projectiles and actinide targets has contributions from processes, such as compound nucleus fission, transfer-induced fission, and noncompound nucleus fission. Mass distribution and mass-dependent anisotropy can be used to identify and delineate the contributions due to these different processes.
Purpose: Mass distribution in $^{28}Si + ^{232}Th$ has been studied at beam energies of 180 and 158 MeV to investigate the nature of mass distribution arising from complete and incomplete momentum-transfer fission events. Mass-dependent angular anisotropy has been measured at 166 MeV to investigate the dominant noncompound nucleus process contributing to the fission.
Method: Mass distribution and mass resolved angular distribution of fission products were measured by the recoil catcher method followed by off-line γ-ray spectrometry.
Results: Mass distributions for full momentum-transfer fission processes were found to be symmetric, and those for transfer-induced fission were found to be asymmetric at both beam energies. The relative contribution from transfer-induced fission was found to be higher at lower beam energy. The anisotropy of the fission product angular distribution was found to increase with decreasing mass asymmetry.
Conclusions: The mass distribution indicates that, apart from the full momentum-transfer fission process, there is a significant contribution due to transfer-induced fission. The mass dependence of angular anisotropy indicated that preequilibrium fission is the dominant noncompound nucleus process in the present reaction system at near barrier energy ($E_{c.m.}/V_C = 1.06$).

DOI: 10.1103/PhysRevC.95.014612

I. INTRODUCTION

Mass distribution and mass resolved angular distribution are important observables to understand the role of the fusion-fission potential-energy landscape in governing the fission process [1]. Mass distribution has a close relationship with the potential-energy landscape of the fissioning nucleus as demonstrated in saddle- and scission-point models [1,2]. In the fission process involving composite systems with $Z \geqslant 100$, stability towards fission mainly comes from shell corrections to the liquid drop model (LDM) potential-energy surface. Due to the compact saddle point and lower fission barrier, such systems are also expected to have contributions from noncompound nucleus (NCN) fission [3–5]. Thus, various NCN fission processes, such as quasifission, preequilibrium fission, and fast fission compete with the compound nucleus fission (CF). In addition, there will be contributions from transfer-induced fission (TF) in reactions involving actinide targets. The contribution from various processes is governed by the entrance channel parameters, such as the target-projectile combination (mass asymmetry) and the projectile energy. Charge and mass distribution studies in such systems would provide information about various fission processes, such as compound nucleus fission, noncompound nucleus fission, and transfer-induced fission, which would help in understanding the fusion-fission process in heavy-ion collisions forming composite systems in the heavy and *trans*-actinide region. In TF, a fissioning nucleus is formed after transfer of a few nucleons from the projectile to the target which subsequently undergoes fission. As seen in earlier studies [6,7], these TF events could be delineated from the full momentum-transfer (FMT) fission events based on the A/Z of the fission products. But the mass distribution for full momentum-transfer fission may have contributions from various NCN processes in addition to CF, which is difficult to delineate.

Fission fragment angular distribution is a sensitive probe for investigating the contribution from noncompound nucleus fission. Mass resolved angular distribution of fission products offers the possibility to distinguish the NCN fission process, namely, preequilibrium fission [8] and quasifission [9]. Both NCN processes lead to an anomalous fission fragment angular distribution. The two processes differ in the fact that, in the case of preequilibrium fission, the fissioning system reaches inside the unconditional saddle point, whereas, in the case of quasifission, the fissioning system escapes into the exit channel without being captured inside the unconditional saddle point. In earlier studies of mass resolved angular distribution in $^{16}O + ^{232}Th$ [10] and $^{20}Ne + ^{232}Th$ [11] reactions, angular anisotropy was observed to increase with decreasing asymmetry of mass division. This could be explained after including the contribution from preequilibrium fission [11,12]. The contribution from preequilibrium fission increases with decreasing mass asymmetry due to a decrease in the fission time scale arising from the reduction in the fission barrier with decreasing mass asymmetry in the vicinity of the saddle point. These observations suggest that the fissioning system reaches inside the saddle point at above barrier energies in

*Corresponding author: suparna@barc.gov.in

these reaction systems. It is important to extend these studies to heavier projectiles to investigate which of the two NCN fission processes is dominant. In the case of heavier projectiles forming a composite system in the transactinides region, the composite system may not reach inside the unconditional saddle point, even if the beam energy is slightly above the entrance channel Coulomb barrier.

In order to investigate the contributions from NCN fission and transfer-induced fission, charge, mass, and mass resolved angular distribution studies were carried out in the ^{28}Si + ^{232}Th reaction by radiochemical method. Charge and mass distribution measurements were carried out at $E_{\rm lab} = 158$ and 180 MeV which correspond to $E_{\rm c.m.}/V_{\rm C} = 1.0$ and 1.17, respectively, where $E_{\rm c.m.}$ and V_C are the projectile energy in the center-of-mass (c.m.) frame of reference and the entrance channel Coulomb barrier, respectively. This projectile-target combination will produce a composite system that may undergo fission with different mechanisms. In the present paper, the contributions from full and partial momentum-transfer fission events to the experimental mass distribution have been determined. The mass-dependent angular anisotropy was measured at $E_{\rm lab} = 166$ MeV (in between the two energies of mass distribution studies), corresponding to $E_{\rm c.m.}/V_C = 1.06$ to investigate the dominant NCN-fission process.

II. EXPERIMENTAL DETAILS

A. Mass distribution measurement

Experiments were carried out at the Bhabha Atomic Research Centre-Tata Institute of Fundamental Research (BARC-TIFR) Pelletron-LINAC facility, Mumbai. For the mass distribution measurement, a self-supporting target of ^{232}Th (thickness of 1.6 mg/cm^2) was bombarded with ^{28}Si beam having energies of 182.5 and 160 MeV. The average energies at the center of the target were 180 and 158 MeV, respectively. Fission products recoiling out of the target were collected in superpure aluminum catcher foils with thicknesses of 6.75 mg/cm^2. A schematic of the irradiation setup is shown in Fig. 1. The catcher foil in the backward direction was mounted on an aluminum cone with a 5-mm hole at the vertex to avoid beam energy degradation in the catcher foil. Irradiations were carried out for a period of about 10 h at higher beam energy and for 17 h at lower beam energy. After irradiation, γ-ray activity of the fission products in different catcher foils and the target were separately assayed using a precalibrated high-purity germanium (HPGe) detector. The decay of the products was followed for nearly 2 months. The unambiguous identification of the fission products was performed based on their characteristic γ rays and half-lives. Nuclear data of fission products for the present paper were taken from Refs. [13,14] and are given in Table I. The γ-ray spectra were analyzed using the peak area analysis software PHAST [15]. Peak areas of the characteristic γ-rays were used to obtain the "end of irradiation activities (A_i)" of the fission products and evaporation residues which were used to obtain the formation cross sections (σ) using the standard activation equation,

$$\sigma = \frac{A}{N\phi(1 - e^{-\lambda T_{\rm irr}})a_\gamma \varepsilon_\gamma}, \tag{1}$$

where N is the number of target atoms per unit area, ϕ is the average number of beam particles incident on the target per unit time, λ is the decay constant of the fission product or evaporation residue, a_γ is the emission probability of a γ ray with energy E_γ, and ε_γ is the full energy detection efficiency at energy E_γ.

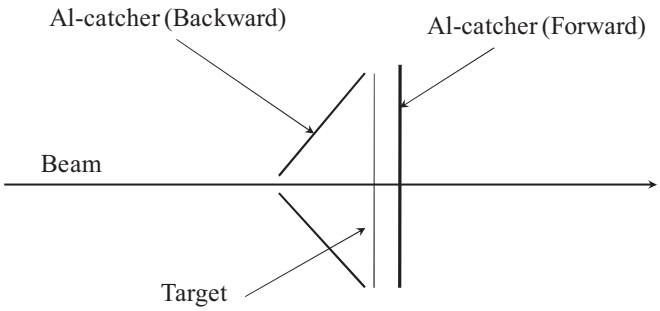

FIG. 1. Schematic of the target catcher assembly for the mass distribution measurement.

B. Angular distribution measurement

For the mass resolved angular distribution measurement, a self-supporting target of ^{232}Th with a thickness of 1.5 mg/cm^2 was irradiated with ^{28}Si beam at a beam energy of 170 MeV. The measurement was performed at a beam energy which was intermediate between the two energies at which the mass distributions were measured. The target was mounted at 45° with respect to the beam direction, so the average energy at the center of the target was 166 MeV. Irradiation was carried out for about 58 h. The recoiling fission products emitted in the forward hemisphere were collected in an aluminum foil with a thickness of 6.75 mg/cm^2 mounted on the inner wall of a cylindrical chamber with the length of 130 mm and a diameter of 146 mm [10]. The foil covered a laboratory angular range of 90°–2.2° and an azimuthal angular range of 0°–180°. After the irradiation the catcher foils were cut into ten strips of width around 20 mm, and each strip corresponding to different $\theta_{\rm lab}$'s was assayed for the activity of the fission products using a HPGe detector coupled to a PC- based multichannel analyzer. γ spectra were analyzed using the spectrum analysis software PHAST [15] to obtain the peak areas under the characteristic γ-ray energy peaks of the fission products. After correcting the peak areas for the decay of the fission products after the irradiation and during counting, their activities at the end of the irradiation were obtained. The yield of a fission product in a given strip "i"(σ_i) was calculated from its end of irradiation activity [Eq. (1)].

The yields of fission products in different strips were corrected for the solid angle using the following equation to obtain the fission product angular distributions in laboratory frame of reference:

$$W(\theta_{\rm lab}) = \frac{\sigma}{\pi[\cos(\theta_{\rm 1lab}) - \cos(\theta_{\rm 2lab})]}, \tag{2}$$

where σ is the yield of the fission product in a given strip, $\theta_{\rm 1lab}$ and $\theta_{\rm 2lab}$ are the angles corresponding to the edges of the strip.

TABLE I. Decay data and formation cross sections of fission products and evaporation residues at $E_{lab} = 180$ and 158 MeV. The decay data were taken from Refs. [13,14]. Cumulative cross sections are represented by (C), and independent cross sections are represented by (I).

Serial No.	Nuclide	Half-life	E_γ (keV)	Intensity (%)	Formation cross section (mb)	
					$E_{lab} = 180$ MeV	$E_{lab} = 158$ MeV
1	^{78}As	1.51 h	694.9	16.7	5.8 ± 1.3 (C)	
2	^{78}Ge	88 min	277.3	96.0	1.10 ± 0.12 (C)	
3	^{85}Kr^{m}	4.48 h	151.2	75.0	4.3 ± 0.2 (C)	1.34 ± 0.21 (C)
4	^{87}Kr	76.3 min	402.6	49.6	5.6 ± 1.1 (C)	1.81 ± 0.33 (C)
5	^{88}Kr	2.84 h	196.5	25.4	5.3 ± 0.4 (C)	2.03 ± 0.36 (C)
6	^{89}Rb	15.4 min	1031.9	58.0	10.4 ± 1.4 (C)	
7	^{90}Y	3.19 h	479.5	90.7	1.8 ± 0.2 (I)	
8	^{91}Sr	9.63 h	749.8	23.6	8.0 ± 1.2 (C)	2.07 ± 0.65 (C)
9	^{92}Sr	2.71 h	1383.9	90.0	10.0 ± 1.1 (C)	
10	^{94}Y	18.7 min	918.7	56.0	5.8 ± 0.8 (C)	
11	^{95}Zr	64.02 d	756.7	54.5	10.7 ± 1.1 (C)	3.28 ± 0.33 (C)
12	^{97}Zr	16.74 h	743.4	93.1	12.5 ± 1.2 (C)	
13	^{98}Nb^{m}	51.3 min	787.4	93	4.4 ± 0.5 (C)	0.88 ± 0.13 (C)
14	^{99}Mo	65.94 h	140.5	90.7	12.0 ± 1.0 (C)	2.17 ± 0.26 (C)
15	^{103}Ru	39.25 d	497.1	90.9	14.6 ± 0.8 (C)	1.96 ± 0.24 (C)
16	^{104}Tc	18.3 min	358.0	89.0	6.5 ± 0.6(I)	
17	^{105}Ru	4.44 h	724.2	46.7	10.5 ± 0.8 (C)	1.54 ± 0.36 (C)
18	^{106}Rh^{m}	131 min	1045.7	30.3	3.3 ± 0.5 (I)	
19	^{107}Rh	21.7 min	302.8	66.0	15.4 ± 2.1 (C)	
20	^{111}Pd^{m}	5.5 h	172.2	34.0	5.2 ± 1.4 (I)	
21	^{112}Pd	21.0 h	617.4	50.0	7.00 ± 0.02 (C)	
22	^{112}Ag	3.14 h	617.4	43.0	7.22 ± 0.03 (I)	
23	^{113}Ag^{g}	5.37 h	298.6	10.0	13.6 ± 1.7 (C)	
24	^{116}In^{m}	54.41 min	1293.5	84.4	6.0 ± 0.5 (I)	
25	^{117}Cd^{m}	3.36 h	552.9	125.0	5.3 ± 0.8 (C)	0.91 ± 0.23 (C)
26	^{117}In^{m}	1.94 h	553	74.8	10.2 ± 0.8 (C)	1.96 ± 0.22 (C)
27	^{118}Sb	5 h	253.7	98.0	1.4 ± 0.1 (I)	
28	^{120}Sb	5.76 d	197.3	87.0	4.3 ± 0.6 (I)	
29	^{122}Sb	2.7 d	564	69.3	7.7 ± 0.6 (I)	0.90 ± 0.16 (I)
30	^{124}Sb^{g}	60.2 d	602.7	97.8	4.1 ± 0.4 (I)	
31	^{124}I	4.18 d	602.7	61.0	3.5 ± 0.5 (I)	
32	^{126}I	13.02 d	388.6	32.2	8.8 ± 1.1 (I)	
33	^{126}Sb^{g}	12.46 d	414.8	83.2	1.94 ± 0.4 (I)	
34	^{127}Xe^{g}	36.41 d	202.9	68.3	4.8 ± 0.5 (I)	
35	^{128}I	25 min	442.9	16.9	9.4 ± 2.3 (I)	
36	^{130}I^{g}	12.36 h	536.1	99.0	2.1 ± 0.2 (I)	0.48 ± 0.08 (I)
37	^{131}I	8.02 d	364.5	81.7	5.5 ± 0.6 (C)	1.40 ± 0.22 (C)
38	^{132}Te	3.204 d	228.2	88.0	3.3 ± 0.3 (C)	0.92 ± 0.18 (C)
39	^{133}I^{g}	20.8 h	529.9	87.0	4.6 ± 0.4 (C)	1.17 ± 0.29 (C)
40	^{133}Ba^{m}	38.9 h	275.9	17.5	6.8 ± 0.8 (I)	
41	^{134}I	52.6 min	847	95.4	6.7 ± 0.9 (C)	1.75 ± 0.26 (C)
42	^{139}Ba	83.06 min	165.8	23.6	6.7 ± 0.6 (C)	
43	^{140}Ba	12.75 d	537.3	24.4	3.34 ± 0.55 (C)	
44	^{140}La	1.68 d	487	45.5	3.6 ± 0.8 (C)	
45	^{141}Ce	32.5 d	145.4	48.2	12.5 ± 1.5 (C)	3.42 ± 0.63 (C)
46	^{142}La	91.1 min	641.2	47.4	4.5 ± 0.6 (C)	1.11 ± 0.18 (C)
47	^{143}Ce	33.04 h	293.27	42.8	4.7 ± 0.4 (C)	1.55 ± 0.26 (C)
48	^{150}Pm	2.68 h	333.9	68.0	2.3 ± 0.5 (I)	
49	^{171}Lu	8.24 d	739.8	47.8	4.0 ± 0.4 (C)	
50	^{172}Lu	6.7 d	1093.6	62.5	3.3 ± 0.4 (I)	
51	^{173}Hf	23.6 h	123.7	83.0	1.07 ± 0.09 (C)	
52	^{232}Pa	1.31 d	894.3	19.8	13.3 ± 0.9	6.6 ± 2.2
53	^{233}Pa	26.97 d	312.17	38.6	26.6 ± 3.1	22.2 ± 4.5

The yields in the eighth and the ninth foils close to 90° were combined.

III. RESULTS AND DISCUSSION

A. Mass distribution at $E_{lab} = 180$ MeV

At $E_{lab} = 180$ MeV, formation cross sections of the fission products were obtained by adding their cross sections in the forward and backward catcher foils and in the target. For a few products, the yields were missing either in the backward or in the forward catcher foils. So the ratio of the yields in the forward-to-backward catcher foils of the remaining products were plotted as a function of mass number to obtain a correlation between the "forward-to-backward ratio (*F/B*)" and the mass number of the fission product (A). From this correlation, the missing yields in the forward or backward catcher foil were calculated. The formation cross sections of 51 fission products are given in Table I. Because of the 5-mm annular hole in the backward catcher, the total cross sections are underestimated by ∼4%. The independent (IN) and cumulative (CU) cross sections are marked by "I" and "*C*," respectively, in the table. The uncertainties on the formation cross sections are quoted at one σ level.

In order to obtain the mass distribution, formation cross sections of the fission products need to be corrected for the charge distribution. The yield $Y(A)$ of a mass chain A is calculated using the IN(A,Z) or CU(A,Z) cross sections of the fission product with mass A and atomic number Z using the following equations:

$$Y(A) = \mathrm{IN}(A,Z)/\mathrm{FIY}(A,Z), \tag{3}$$

$$Y(A) = \mathrm{CU}(A,Z)/\mathrm{FCY}(A,Z), \tag{4}$$

where FIY(A,Z) and FCY(A,Z) are the fractional independent and cumulative yields, respectively, of the measured fission product having mass number A and atomic number Z. FIY(A,Z) and FCY(A,Z) are given by the following equations:

$$\mathrm{FIY}(A,Z) = \frac{1}{\sqrt{2\pi\sigma_Z^2}} \int_{Z-0.5}^{Z+0.5} e^{-(Z-Z_P)^2/2\sigma_Z^2} dZ, \tag{5}$$

$$\mathrm{FCY}(A,Z) = \frac{1}{\sqrt{2\pi\sigma_Z^2}} \int_{-\infty}^{Z+0.5} e^{-(Z-Z_P)^2/2\sigma_Z^2} dZ, \tag{6}$$

where σ_Z and Z_P are the width and the most probable charge, respectively, for the isobaric yield distribution. Thus, calculation of the mass yield for a mass chain with mass number A from the experimentally determined yield of a fission product $[Y(A)]$ requires the information about the Z_P and σ_Z of the isobaric yield distribution for the mass chain with mass number A. Ideally, independent yields of at least three members in the isobaric chain are required to obtain these charge distribution parameters. However, in general, it is difficult to measure three independent yields in an isobaric chain, and an alternative approach is generally used to obtain the charge distribution parameters as discussed in the next section.

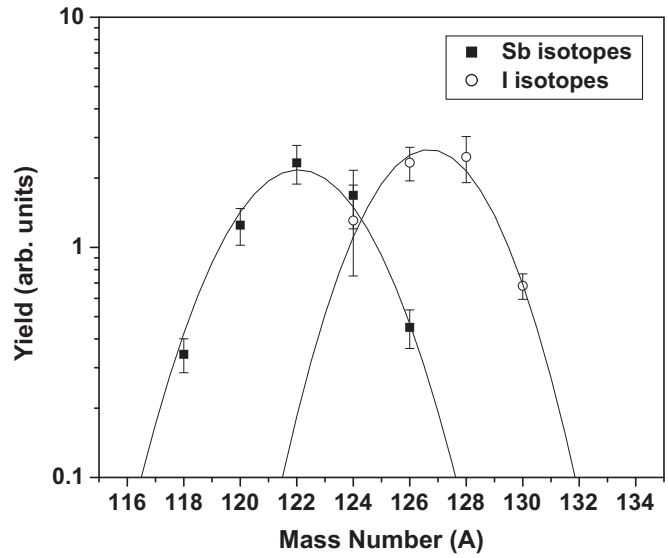

FIG. 2. Plot of independent yields of Sb and I isotopes at $E_{lab} = 180$ MeV.

B. Charge distribution parameters

Isotopic yield distributions of the elements formed in the fission can be used to obtain the charge distribution parameters. In this case, the independent yields of various isotopes of Sb(^{118,120,122,124,126}Sb) (where Sb represents antimony) and I(^{124,126,128,130}I) (where I represents iodine) in the backward catcher foil were used. The measured yields of Sb isotopes were taken as independent as measured isotopes did not have any precursor contribution. The measured yield of ^{124}Sb was corrected for the incomplete decay of its high spin isomer to the measured isotope. In the case of iodine isotopes, measured cross sections of ^{124,126,128,130}I isotopes were independent as there was no precursor contribution for these isotopes. The measured independent yields of all Sb and I isotopes are plotted as a function of mass number and shown in Fig. 2. It is clear from the figure that yields of the Sb isotopes could be fitted to one Gaussian, indicating their formation in the CF process. Similar results were obtained for I isotopes up to mass 130. The FIYs of Sb($A = 118-126$) and I($A = 124-130$) isotopes are plotted as a function of the A/Z of these isotopes as shown in Fig. 3. The data could be fitted to a Gaussian, and the value of the most probable $A/Z\{(A/Z)_P\}$ was obtained as 2.391 ± 0.022. The uncertainty quoted on the parameter is the fitting error. Based on the unchanged charge distribution hypothesis, the most probable charge Z_P for a particular mass chain with mass number$A$ was obtained as

$$Z_P(A) = \frac{A}{\left(\frac{A}{Z}\right)_P}. \tag{7}$$

Thus, $Z - Z_P$ was obtained for each mass number of the Sb and I isotopes, and the fractional independent yields were then plotted as a function of $Z - Z_P$. The data were fitted to a Gaussian as shown in Fig. 4, and the value of σ_Z was obtained as 0.87 ± 0.23. The charge distribution parameters, thus obtained, were used for the charge distribution correction of the experimental yields of different fission products. $(A/Z)_P$

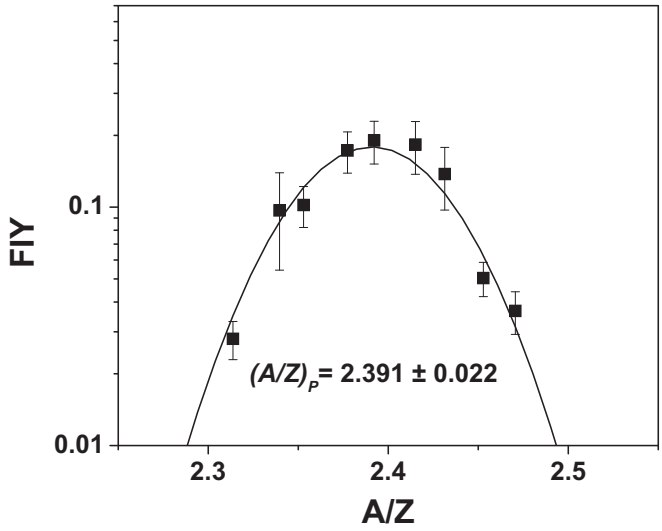

FIG. 3. Fractional independent yield (FIY) of Sb and I isotopes as a function of their A/Z at $E_{\rm lab} = 180$ MeV.

is related to the mass ($A_{\rm CN}$) and charge ($Z_{\rm CN}$) of the compound nucleus by the following equation:

$$\left(\frac{A}{Z}\right)_P = \frac{A_{\rm CN} - \nu_T}{Z_{\rm CN}}, \tag{8}$$

where ν_T is the average number of neutrons emitted during the fission process. The value of ν_T, calculated using Eq. (8), was found to be 11.3, which was in reasonable agreement with the value of 10.1, calculated using the prescription of Kozulin *et al.* [16]. Z_P values for various mass chains obtained using $(A/Z)_P$ from Eq. (8) were used for the charge distribution correction using Eqs. (3)–(6).

C. Mass distribution

The experimental formation cross sections of the fission products were corrected for charge distribution using the

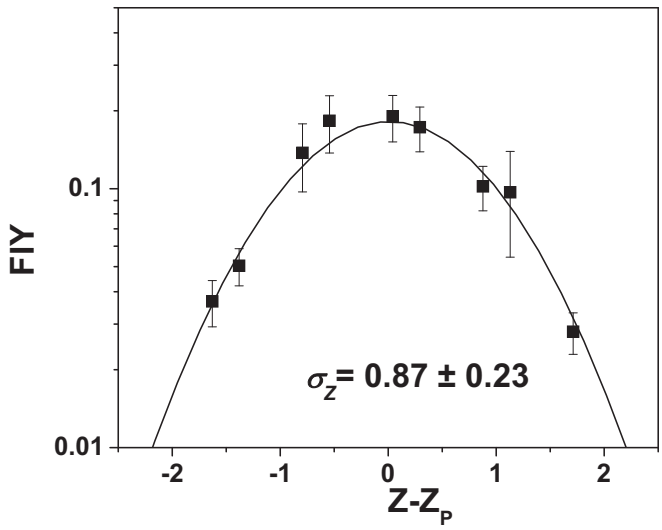

FIG. 4. Fractional independent yield (FIY) of Sb and I isotopes as a function of corresponding $Z - Z_P$ values at $E_{\rm lab} = 180$ MeV.

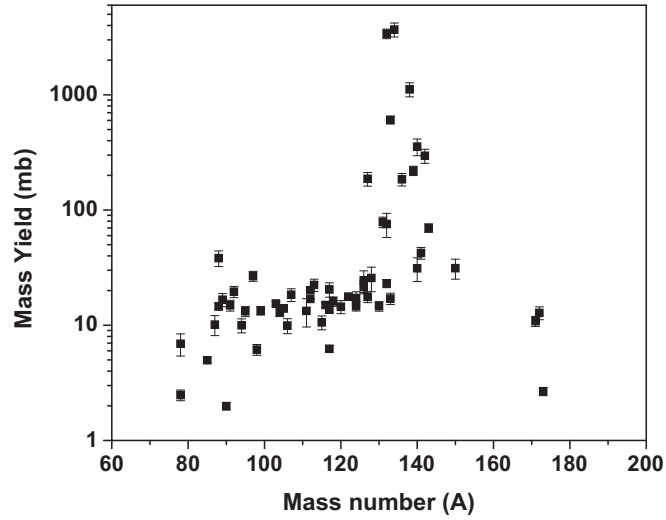

FIG. 5. Mass yields of the fission products as a function of their mass number at $E_{\rm lab} = 180$ MeV.

parameters $(A/Z)_P$ and σ_Z. Figure 5 shows the plot of charge distribution corrected mass yields as a function of mass number. As can be seen from the figure, most of the fission product mass yields fall on a Gaussian distribution, indicating their formation from the FMT fission process. For some products in the higher mass region ($A = 127-142$), very high yields were obtained after the charge distribution correction. This indicated that these products are predominantly formed in TF where the fissioning nucleus is targetlike and has higher A/Z compared to that for the FMT fission. Experimentally measured fission products in the heavy mass region are close to the β stability valley, which shifts to higher A/Z with increasing mass. Therefore, these products are expected to have substantial contributions from TF for which the fissioning system is having higher A/Z. This is further confirmed when the charge distribution corrected mass yields are plotted as a function of A/Z of the products. As seen in Fig. 6, very high yields of the products with $A/Z > 2.47$ shows that they have significant contributions from the TF process.

The neutron-deficient products, such as ^{118,120,122,124,126}Sb, ^{124,126,128,130}I, ^{116}In, ^{117}In^m, ^{127}Xe, ^{117}Cd^m, ^{173}Hf, and ^{133}Ba, are presumed to be predominantly formed in FMT fission. Independent yields of ^{171}Lu, ^{172}Lu, ^{112}Ag, and ^{111}Pd^m also are having major contributions from FMT fission. ^{85}Kr^m will have negligible contributions from TF as contributions of TF to very asymmetric masses will be very low. The yields of these 20 fission products were corrected for charge distribution using the parameters for FMT fission. The same yields also were assigned to mass numbers corresponding to $A_{\rm CN}$-ν_T-A_F to get the complementary masses, where A_F is the mass of the fission product. Then, the mass yields and the reflected points were fitted to a Gaussian distribution. The data points along with the reflected points (yields assigned to complementary masses) are shown in Fig. 7. The fitted Gaussian is shown as a black line. The variance of the mass distribution was found to be 687 ± 53 u^2. This value is comparable to those observed in other reaction

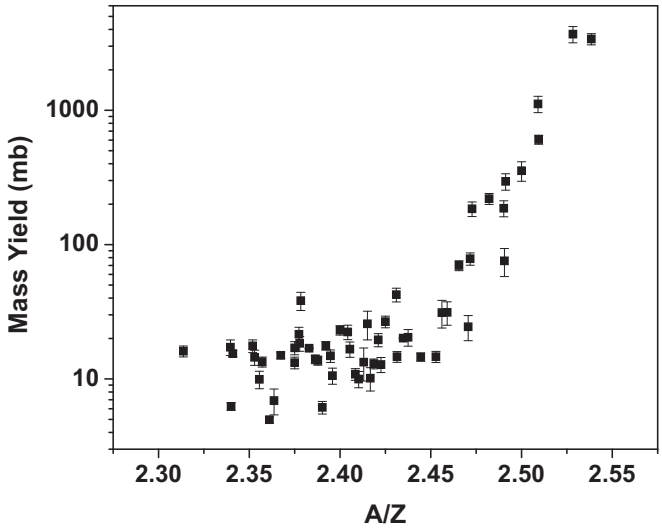

FIG. 6. Mass yields of the fission products as a function of their A/Z at $E_{\rm lab} = 180$ MeV.

systems where similar fissioning systems were produced with similar average angular momentum $\langle l \rangle$ and saddle-point temperatures ($T_{\rm saddle}$) [17–19]. In order to obtain the yields of the fission products in transfer-induced fission, the cumulative [CU(A)] and independent [IY(A)] yields of different fission products formed in FMT fission were estimated using mass yields $Y(A)$ from the fitted Gaussian in Eqs. (3) and (4). The difference between the estimated FMT fission yields and the experimental yields was the contribution from TF. A charge distribution correction appropriate for TF is to be performed to obtain the TF mass distribution.

Since the fissioning system in TF will be the result of the transfer of a few nucleons to the target nucleus, it will be having mass close to the fissioning system formed in TF in

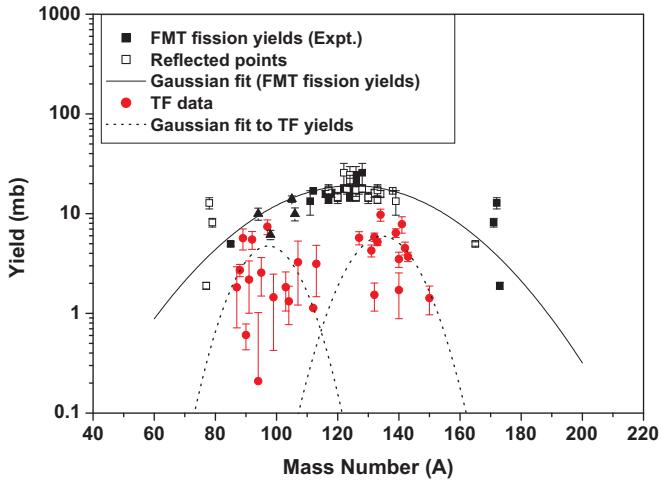

FIG. 7. Mass distribution in the ^{28}Si + ^{232}Th reaction at $E_{\rm lab} =$ 180 MeV. The experimental FMT fission mass yield (■) and the reflected data (□) are fitted to a Gaussian distribution (solid line). The extracted TF mass yield data (●) are fitted to two Gaussians (dotted line). (▲) are FMT fission yields not used in the Gaussian fitting (see the text for details).

^{19}F + ^{232}Th and ^{20}Ne + ^{232}Th reactions. Hence, the charge distribution parameters for TF were taken as the same as used in these systems [6,7]. The value of $(A/Z)_P$ was taken as 2.52 from Ref. [6]. The value of σ_Z was taken as 0.7 from Ref. [20]. The resulting mass distribution obtained using the charge distribution parameters for TF was observed to be asymmetric.

The TF mass distribution, thus obtained, is also plotted in Fig. 7. The FMT fission mass yields are shown with squares, and the TF mass yields are shown with circles. A few data points, having A/Z close to TF products, were not included in the FMT fission Gaussian fitting. But, for these products, the TF yield was negligible, and the entire cross section was attributed to FMT fission. These are represented by triangles. The symmetric nature of the FMT fission mass distribution is expected due to the vanishing of shell effects at higher excitation energies. The best-fit value of the centroid is 125.0 ± 0.5 u. This corresponds to a ν_T value of 10 ± 1, which is consistent with the $(A/Z)_P$ value used for FMT fission charge distribution. The FMT fission cross section obtained is 627 ± 19 mb. The uncertainty quoted is the fitting error. The coupled channel calculations were carried out using the code CCFUS [21], and the fusion cross section was calculated as 668 mb. The estimate of the TF cross section was obtained by fitting the mass distribution to two Gaussians. The centroid values were obtained as 97.3 ± 1.8 and 134.6 ± 2.1 u. The total TF cross section was found to be 123 ± 20 mb, which was about 16% of the total fission cross section.

D. Mass distribution at $E_{\rm lab} = 158$ MeV

At $E_{\rm lab} = 158$ MeV, the formation cross sections of 22 fission products were obtained from the cross section in the backward catcher foil. The total formation cross section required the information about the cross section in the forward direction. For this, the cross section in the backward catcher was corrected to account for the emission in the forward hemisphere. For this correction, the forward-to-backward ratio was obtained using the standard kinematic equations with fission fragment kinetic energies obtained using the prescription of Rossner *et al.* [22]. The forward-to-backward ratios were calculated for the events resulting from complete momentum transfer. Fission fragment masses were transformed into the corresponding product masses after correcting for the neutrons evaporated in the fission process, which were calculated using the prescription of Kozulin *et al.* [16]. The number of evaporated neutrons was apportioned according to the fission fragment mass ratios. From the forward-to-backward ratio, the correction factors for the emission of fission products in the forward hemisphere were calculated. The total yields, thus obtained, were underestimated by about 7% due to the 5-mm annular hole in the backward catcher. The total cross sections are given in Table I. The independent and cumulative cross sections are marked by *I* and *C*, respectively, in the table. The uncertainties on the formation cross sections are quoted at one σ level.

Since yields of only four neutron-deficient fission products (mainly produced in FMT fission), namely, ^{117}In^m, ^{117}Cd^m, ^{122}Sb, and ^{130}I^g were obtained, it was difficult to

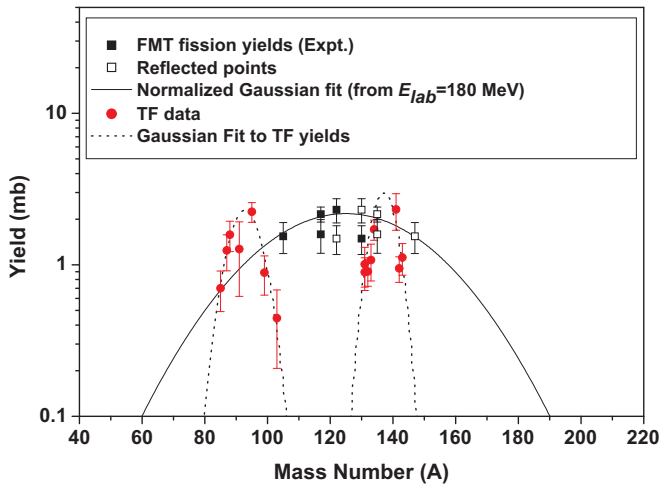

FIG. 8. Mass distribution at $E_{\rm lab} = 158$ MeV. The solid line is the FMT fission mass distribution obtained by normalizing the FMT fission mass distribution fit at higher beam energy (see text for details). The dotted lines are Gaussian fits to the extracted TF mass yields.

fit to a Gaussian to get the FMT fission mass distribution. As the yields of a sufficient number of isotopes for a given element could not be measured, the σ_Z value was taken as 0.87 for carrying out the charge distribution correction. This is the same value as used for the higher-energy data. This is a good approximation as the σ_Z value is nearly constant in the moderate excitation energy range. The most probable $A/Z\{(A/Z)_P\}$ was obtained using Eq. (8) and the ν_T value obtained using the prescription of Kozulin *et al.* [16]. The nature of the FMT fission mass distribution is expected to be similar to that at higher beam energy. The products around the symmetric region (^{122}Sb and ^{130}I^g) are expected to be produced mainly in FMT fission. The average of the ratio of FMT fission mass yields at $E_{\rm lab} = 180$ and 158 MeV for $A = 122$ and 130 was obtained as 8.77. The fitted FMT fission mass distribution obtained at $E_{\rm lab} = 180$ MeV was normalized by this factor to get the FMT fission mass distribution at lower energies. Based on this normalization, the FMT fission cross section was obtained as 71 ± 2 mb. The contribution of TF in the formation cross section of the remaining fission products was obtained in a similar way as performed at the higher beam energy. The cross section of ^{105}Rh showed no contribution from TF. All the experimental data points for FMT fission and TF mass distribution are plotted as a function of mass number and shown in Fig. 8 along with the normalized fit to the FMT fission mass distribution at the higher beam energy. As seen from the figure, the TF mass distribution shows two distinct peaks indicating the asymmetric nature of the mass distribution similar to that observed at higher beam energy. The TF mass distribution was fitted into two Gaussians. The two asymmetric peaks, when fitted, gave centroid values as 92.8 ± 0.4 and 136.8 ± 0.3 u. The TF cross section was found to be 30 ± 2 mb. The quoted uncertainties are fitting errors. This is about 30% of the total fission cross section at this beam energy, which is higher as compared to that observed at the higher beam energy. This could be due to a larger decrease in the FMT fission cross section than the TF cross section at the beam energy close to the barrier. The cross section of the evaporation residues formed in this reaction, namely, ^{233}Pa (p transfer) and ^{232}Pa (p transfer followed by n emission), were also measured at both energies and are given in Table I.

E. Mass resolved angular distribution

The laboratory angular distributions were transformed into c.m. frame of reference assuming complete momentum transfer and using the fission fragment kinetic energies obtained using the prescription of Rossner *et al.* [22]. As was observed in the mass distribution at two different beam energies, there is a significant contribution from TF involving incomplete momentum transfer. Fission products in the asymmetric mass region and with higher A/Z are likely to have significant contributions from TF. As seen in Fig. 6, the products with $A/Z > 2.47$ were having predominant contributions from TF. There may be a contribution from TF to fission products even with lower A/Z due to the decay of the comparatively more neutron-rich precursor, although the relative contribution will be comparatively less in this case.

The c.m. angular distributions were fitted using

$$W(\theta_{\rm c.m.}) = a + b\ \cos^2\theta_{\rm c.m.}, \tag{9}$$

where $\theta_{\rm c.m.}$ is the c.m. angle and a and b are variable parameters. The experimental data with the respective linear fit are shown in Fig. 9. Angular distributions of fission products with $A/Z > 2.47$ are shown as hollow circles. It should be mentioned here that including higher-order terms for fitting gave similar results for many nuclides but the error on the parameters was large. Therefore, linear fitting (shown as the solid lines in Fig. 9) was selected for the determination of angular anisotropies. From the linear fits, angular anisotropies were obtained as

$$\frac{W(0)}{W(90)} = 1 + \frac{b}{a}. \tag{10}$$

The values of angular anisotropies of different fission products were plotted as a function of their masses and are shown in Fig. 10. The uncertainties on the angular anisotropy values are due to the fitting error. Dependence of angular anisotropy of different fission products on their masses can clearly be seen from the figure with the symmetric products having higher anisotropy as compared to the asymmetric ones. This observation is similar to that in earlier studies on mass resolved angular distribution in ^{16}O + ^{232}Th [10] and ^{20}Ne + ^{232}Th [11] reactions. This suggests preequilibrium fission to be the dominant NCN-fission process. However increase in the anisotropy values in the symmetric region is larger compared to that observed in earlier studies [10,11]. This may be due to the larger contribution from preequilibrium fission owing to the smaller fission barrier and larger average angular momentum of the fissioning nucleus in the present study. This also results in the larger average angular anisotropy (2.37 ± 0.16) as compared to that observed in earlier studies at similar values of $E_{\rm c.m.}/V_{\rm C}$. While calculating the average anisotropy, anisotropy values of different fission products were weighted for their mass yields. The yield data were taken from

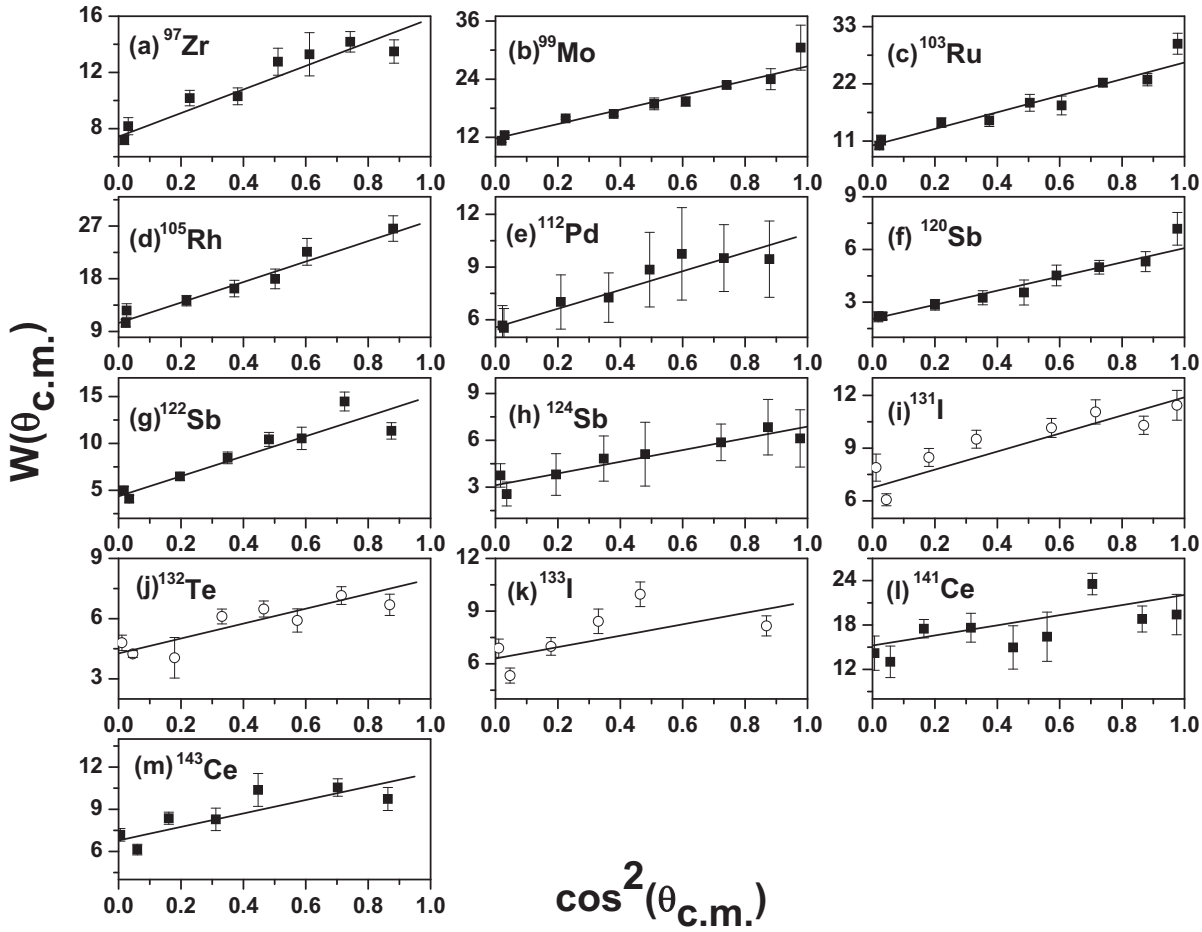

FIG. 9. (a)–(m) Angular distributions of different fission products in $^{28}\mathrm{Si} + ^{232}\mathrm{Th}$ at $E_{\mathrm{lab}} = 166$ MeV. The products formed in FMT fission are shown as solid squares (■). (i)–(k) The products with $A/Z > 2.47$, formed mainly in TF, are shown with open circles (◯).

the mass distribution at 180 MeV as the width of the mass distribution is not expected to change significantly unless the beam energy is very close to the entrance channel Coulomb barrier. Theoretical calculation of the mass-dependent angular anisotropy requires the mass asymmetry-dependent LDM barrier energies [12]. However, the composite system in the present reaction is on the verge of nuclear stability as predicted by the LDM. Therefore, in order to investigate the contribution from NCN fission, a model-independent analysis has been carried out. Based on the statistical saddle-point model, the angular anisotropy and $\langle l^2 \rangle$ are approximately related as [23]

$$\frac{W(0)}{W(90)} = 1 + \frac{\langle l^2 \rangle}{4K_0^2}, \tag{11}$$

where K_0^2 is the variance of the K distribution. The l distribution was calculated using the code CCFUS [17], which gave the $\langle l^2 \rangle$ value as 969 $\hbar^2$. Using this value of $\langle l^2 \rangle$ and the experimental average anisotropy in Eq. (11), the value of K_0^2 was obtained as $177 \pm 12\,\hbar^2$. In the liquid drop model, the fissility of the fissioning system is defined as [24]

$$\chi = \frac{Z^2/A}{50.883\left\{1 - 1.7826\left(\frac{N-Z}{A}\right)^2\right\}}, \tag{12}$$

where Z, N, and A are the proton number, the neutron number, and the mass number of the fissioning nucleus. The fissility value was calculated as 0.88 for the fissioning system formed in the full momentum-transfer events. As the contribution from noncompound nucleus fission is dependent on entrance channel mass asymmetry, the K_0^2 value from the present work was compared with other systems with varying entrance channel mass asymmetry leading to the compound nucleus in the actinide and *trans*-actinide regions with similar $\langle l^2 \rangle$ values and temperatures [11,24–27] as that of the present study. A list of the selected systems along with the relevant data is given in Table II. The plot of K_0^2 as a function of $Z_P Z_T$ is shown in Fig. 11. The errors reported on the data point for the $^{28}\mathrm{Si} + ^{232}\mathrm{Th}$ and $^{20}\mathrm{Ne} + ^{232}\mathrm{Th}$ [11] reactions in the table are deduced from the error on the experimental anisotropy. The solid points represent the data taken from Refs. [11,24–27], and the present data is shown as open circles. As can be seen from the plot, the data get grouped into two categories. The systems having low $Z_P Z_T$ produced with lighter projectiles form one group which lies on the left side of the plot. The second group comprises of those fissioning systems with higher $Z_P Z_T$ that are produced using heavier projectiles, and they lie on the right side of the plot. For the lighter actinide fissioning systems formed using lighter projectiles, the data show that

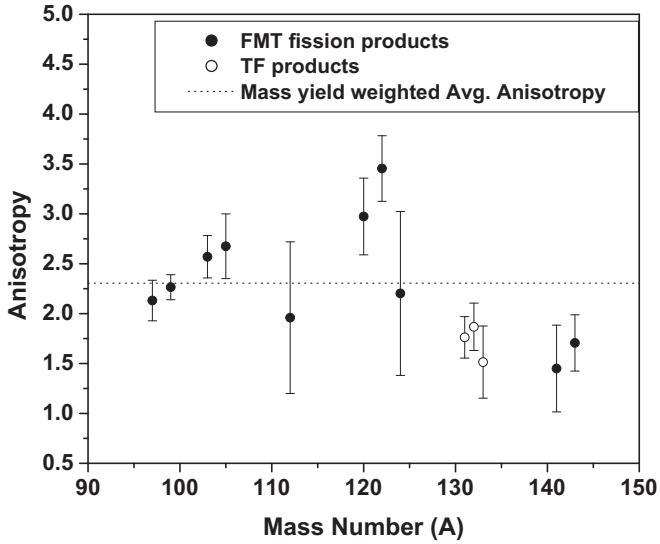

FIG. 10. Anisotropy of different fission products as a function of the mass number of the products. The mass yield weighted average anisotropy is shown as a dotted line.

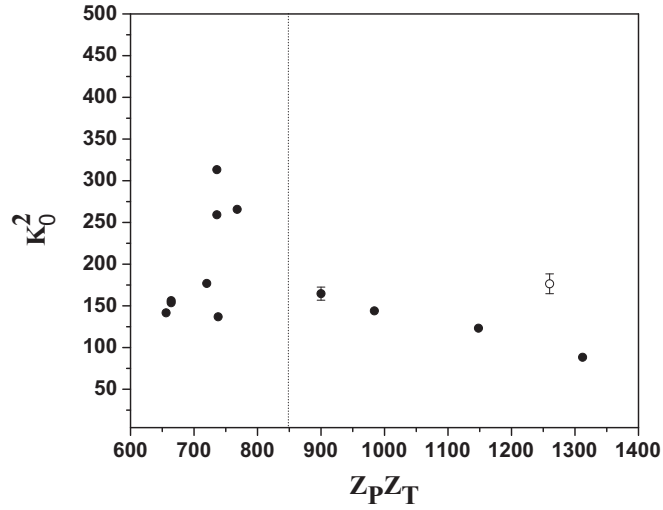

FIG. 11. Comparison of K_0^2 values for various target-projectile combinations leading to fissioning systems in the actinide and *trans*-actinide regions [11,24–27]. The projectile energy, in each case, is chosen such that the $\langle l^2 \rangle$ values and compound nucleus temperature are close to that of the present system. The present experimental data is represented by the open circle (◯).

K_0^2 increases with increasing $Z_P Z_T$. For such systems, as the composite system charge and mass increase, the saddle point becomes more compact. Hence, there will be an increase in the effective moment of inertia (I_{eff}), and hence, K_0^2 would increase. For systems formed using heavier projectiles in the heavy and *trans*-actinide regions, the data show an opposite trend. Based on the extrapolation of the lower $Z_P Z_T$ system with increasing $Z_P Z_T$, K_0^2 will increase, and anisotropy is expected to decrease. But, with increasing $Z_P Z_T$ and the mass of the composite system, the contribution from NCN fission will also increase, which will result in an increase in anisotropy thereby decreasing K_0^2. The net effect of these opposing factors causes K_0^2 to slowly fall as a function of $Z_P Z_T$ as seen in the figure. For example, from Table II, it can be seen that the K_0^2 values for ^{264}Rf (^{16}O + ^{248}Cm) and ^{260}Rf (^{28}Si + ^{232}Th) are 266 $\hbar^2$ and 177 $\hbar^2$, respectively. This clearly shows that a similar system produced by a heavier projectile shows higher anisotropy (lower K_0^2) due to large contributions from NCN processes. The K_0^2 value obtained in the present paper lies in the second group of heavier projectiles. This indicates that, in the present case, there is a significant contribution from NCN fission. The mass-dependent anisotropy results suggest preequilibrium fission to be the dominant NCN process. However, the present data is slightly higher than the adjacent points. This probably could be because the fissility of the composite system is substantially higher than the neighboring systems. The more compact saddle point for the present system

TABLE II. Comparison of K_0^2 values for reaction systems with different target-projectile combinations leading to composite systems in the actinide and *trans*-actinide regions with similar $\langle l^2 \rangle$ values [11,24–27].

Reaction	Compound nucleus	Fissility (χ)	$Z_P Z_T$	E_{lab} (MeV)	$\langle l^2 \rangle$ ($\hbar^2$)	$\frac{W(0^\circ)}{W(90^\circ)}$	K_0^{2a}	Reference
^{16}O + ^{208}Pb	^{224}Th	0.763	656	110	1275	3.13	141.6	[24]
^{16}O + ^{209}Bi	^{225}Pa	0.774	664	102	870	2.48	153.8	[25]
				112	1290	3.05	156.3	[26]
^{16}O + ^{232}Th	^{248}Cf	0.826	720	95	640	1.93	176.9	[24]
^{16}O + ^{238}U	^{254}Fm	0.842	736	96	745	1.62	313.3	[27]
				110	1255	2.24	259.2	[24]
^{16}O + ^{248}Cm	^{264}Rf	0.875	768	110	1145	2.11	265.7	[24]
^{19}F + ^{208}Pb	^{227}Pa	0.771	738	110	970	2.79	136.9	[24]
^{24}Mg + ^{208}Pb	^{232}Pu	0.800	984	140	1035	2.78	144	[24]
^{28}Si + ^{208}Pb	^{236}Cm	0.818	1148	160	1045	3.01	123.2	[24]
^{32}S + ^{208}Pb	^{240}Cf	0.837	1312	185	1005	3.53	88.4	[24]
^{20}Ne + ^{232}Th	^{252}Fm	0.844	900	125.6	968	2.41 ± 0.11	172 ± 8[b]	[11]
^{28}Si + ^{232}Th	^{260}Rf	0.88	1260	166	969	2.37 ± 0.16	177 ± 12[b]	This paper

[a]Taken as a square of the reported values.

[b]Errors reported are deduced from errors on measured anisotropies.

may lead to enhancement of K_0^2, even for the compound nucleus fission.

IV. CONCLUSIONS

Mass distribution and mass resolved angular distribution of fission products were measured in $^{28}\mathrm{Si} + ^{232}\mathrm{Th}$ reaction. Mass distribution was found to be symmetric for CF and asymmetric for incomplete momentum-transfer events, i.e., TF. The contribution from TF was delineated based on the A/Z of the fission products. The relative contribution of TF was found to be more around the barrier than that at the higher beam energy. The mass resolved angular anisotropy measurements at slightly higher beam energy compared to the entrance channel Coulomb barrier showed higher anisotropy for symmetric fragments. This indicated preequilibrium fission to be the dominant noncompound nucleus fission mechanism at above barrier energies.

ACKNOWLEDGMENTS

The authors thank Dr. S. K. Sharma and Dr. P. Maheshwari for their help during the experiment. The authors would also like to thank Dr. K. Sudarshan for valuable discussions. Thanks are due to the operating staff BARC-TIFR Pelletron-LINAC facility, Mumbai for the smooth operation during the experiment.

[1] C. F. Tsang and J. B. Wilhelmy, Nucl. Phys. A **184**, 417 (1972).
[2] B. D. Wilkins, E. P. Steinberg, and R. R. Chasman, Phys. Rev. C **14**, 1832 (1976).
[3] J. Toke, R. Bock, G. X. Dai, A. Gobbi, S. Gralla, K. D. Hildenbrand, J. Kuzminski, W. F. J. Müller, A. Olmi, and H. Stelzer, Nucl. Phys. A **440**, 327 (1985).
[4] K. Nishio, H. Ikezoe, S. Mitsuoka, I. Nishinaka, Y. Nagame, Y. Watanabe, T. Ohtsuki, K. Hirose, and S. Hofmann, Phys. Rev. C **77**, 064607 (2008).
[5] K. Nishio, H. Ikezoe, I. Nishinaka, S. Mitsuoka, K. Hirose, T. Ohtsuki, Y. Watanabe, Y. Aritomo, and S. Hofmann, Phys. Rev. C **82**, 044604 (2010).
[6] G. K. Gubbi, A. Goswami, B. S. Tomar, A. Ramaswami, A. V. R. Reddy, P. P. Burte, S. B. Manohar, and B. John, Phys. Rev. C **59**, 3224 (1999).
[7] S. Sodaye, R. Tripathi, K. Sudarshan, and R. Guin, Phys. Rev. C **87**, 044610 (2013).
[8] V. S. Ramamurthy and S. S. Kapoor, Phys. Rev. Lett. **54**, 178 (1985).
[9] W. J. Swiatecki, Phys. Scr. **24**, 113 (1981).
[10] B. John *et al.*, Phys. Rev. C **51**, 165 (1995).
[11] R. Tripathi, S. Sodaye, K. Sudarshan, and R. Guin, Phys. Rev. C **88**, 024603 (2013).
[12] D. Vorkapić and B. Ivanišević, Phys. Rev. C **55**, 2711 (1997).
[13] R. B. Firestone and V. S. Shirley, *Table of Isotopes*, 8th ed. (Wiley-Interscience, New York, 1999).
[14] U. Reus and W. Westmeier, At. Data Nucl. Data Tables **29**, 1 (1983).
[15] P. K. Mukhopadhyay, in *Proceedings of Symposium on Intelligent Nuclear Instrumentation, Mumbai (2001)*, Vol. 33, p. 307; INIS Repository **33**, 33001318 (2001).
[16] E. M. Kozuline, A. Ya. Rusanov, and G. N. Smirenkin, Phys. At. Nucl. **56**, 166 (1993).
[17] A. Ya. Rusanov, M. G. Itkis, and V. N. Okolovich, Phys. At. Nucl. **60**, 683 (1997); M. G. Itkis, S. M. Luk'yanov, V. N. Okolovich, Yu. E. Penionzhkevich, A. Ya. Rusanov, V. S. Salamatin, G. N. Smirenkin, and G. G. Chubaryan, Sov. J. Nucl. Phys. **52**, 15 (1990).
[18] G. G. Chubaryan, S. M. Luk'yanov, Yu. E. Penionzhkevich, V. S. Salamatin, M. G. Itkis, V. N. Okolovich, A. Ya. Rusanov, and G. N. Smirenkin, Sov. J. Nucl. Phys. **53**, 738 (1991).
[19] W. Q. Shen, J. Albinski, A. Gobbi *et al.*, Phys. Rev. C **36**, 115 (1987).
[20] H. Umezawa, S. Baba, and H. Baba, Nucl. Phys. A **160**, 65 (1971)
[21] C. H. Dasso and S. Landowne, Comput. Phys. Commun. **46**, 187 (1987).
[22] H. H. Rossner, J. R. Huizenga, and W. U. Schröder, Phys. Rev. Lett. **53**, 38 (1984).
[23] R. Vandenbosch and J. R. Huizenga, *Nuclear Fission* (Academic, New York, 1973).
[24] B. B. Back, R. R. Betts, J. E. Gindler, B. D. Wilkins, S. Saini, M. B. Tsang, C. K. Gelbke, W. G. Lynch, M. A. McMahan, and P. A. Baisden, Phys. Rev. C **32**, 195 (1985).
[25] V. E. Viola, Jr., T. D. Thomas, and G. T. Seaborg, Phys. Rev. **129**, 2710 (1973).
[26] S. A. Karamyan, I. V. Kuznetsov, T. A. Muzycka, Yu. Ts. Oganesyan, Yu. E. Penionzkevich, and B. I. Pustyl'nik, Yad. Fiz. **6**, 494 (1967) [Sov. J. Nucl. Phys. **6**, 360 (1968)].
[27] J. Toke, R. Bock, G. X. Dai, A. Gobbi, S. Gralla, K. D. Hildenbrand, J. Kuzminski, W. F. J. Müller, A. Olmi, W. Reisdorf, S. Bjørnholm, and B. B. Back, Phys. Lett. B **142**, 258 (1984).